JOURNAL OF SOLID STATE CHEMISTRY **122,** 273–280 (1996)
ARTICLE NO. 0113

A Crystallographic Contribution to the Mechanism of a Mechanically Induced Solid State Reaction

N. J. Calos,* J. S. Forrester,† and G. B. Schaffer†,[1]

*Centre for Microscopy and Microanalysis, The University of Queensland, Queensland 4072, Australia; and †Department of Mining and Metallurgical Engineering, The University of Queensland, Queensland 4072, Australia

Received July 24, 1995; in revised form December 4, 1995; accepted December 7, 1995

Using X-ray diffraction analysis and Raman spectroscopy techniques, a mechanically induced double displacement reaction has been used to investigate the chemical mechanism by which mechanical alloying occurs. The specific reaction studied was the reduction of cupric oxide by iron. From Rietveld analysis of milled powders, isotropic atomic displacement parameters are refined and the lattice strain involved in displacing oxygen in the CuO lattice is then calculated. In addition, anisotropic atomic displacement parameters are refined, providing information regarding the reaction pathway. Raman spectroscopy is used to differentiate between thermal motion and static displacement of oxygen atoms in the CuO lattice. Using this information, the mechanism of a mechanically induced solid state reaction is described.

INTRODUCTION

Mechanical alloying (MA) is a process which has become widely used since the 1970s (1, 2), but investigations into the mechanism have been somewhat limited. In simple terms, MA can be viewed as a means to induce solid state reactions in powders during ball milling. Acquiring an understanding of how the reaction occurs may allow the possibility of defining systems which suit the MA process.

One aspect of MA which sets it apart from other solid state processes is that it is nominally a room temperature process. Reactions can occur at room temperature during MA because the reactants are severely strained and reaction rates are controlled by the rate of strain accumulation (3, 4). It is generally assumed that the strain is due to the introduction of line and point defects and a reduction in the grain size. The diffusion pathway changes during milling from bulk diffusion to short circuit diffusion. The activation energy is decreased as a consequence (4). It is apparent that the kinetic energy of the balls is transferred to the powders, increasing the lattice energy and decreasing the activation energy. What is unresolved is the nature of the defects which store the excess energy, and how this influences the reaction pathway. The aim of this article is to study the reaction from a crystallographic point of view, and in this way examine strain accumulation in a crystal lattice during a reaction.

Favas *et al.* (5) used anisotropic Gaussian atomic displacement parameters (ADPs) to visualize phase changes in K_2TaF_7. Argyriou (6) isolated static disorder contributions from thermal vibrations in measured ADPs of ZrO_2 in a temperature dependent neutron diffraction study. These examples point to the possibility of following reactions through crystallographic measurements of atomic motion and disorder in the solid state. In this paper we apply this methodology to the mechanically induced reduction of CuO by Fe.

EXPERIMENTAL

Previously (4), cupric oxide and iron had been mechanically alloyed in a SPEX 8000 mixer/mill, and X-ray diffraction (XRD) patterns were collected using a Philips PW1130 diffractometer with a graphite monochromator using Cu$K\alpha$ radiation. These patterns were reanalyzed using the Rietveld refinement computer program LHPM8 (7, 8). Atomic displacement parameters extracted from these refinements were used in the RIETAN-94 computer program to calculate Madelung coefficients (9, 10). These parameters were also used in the program ATOMS V3.1[2] in order to visualize equiprobability ellipsoids for both copper and oxygen ions, and indicate the general reaction pathway. Raman spectra were collected with a Perkin–Elmer 2000R FT-Raman spectrometer, using a NdYAG laser. Unmilled CuO and CuO milled for 36 min using the same milling conditions as the previous work were scanned at room temperature in order to compare their lattice modes. De-

[1] To whom correspondence should be addressed.

[2] Shape Software, E. Dowty © 1995.

0022-4596/96 $18.00

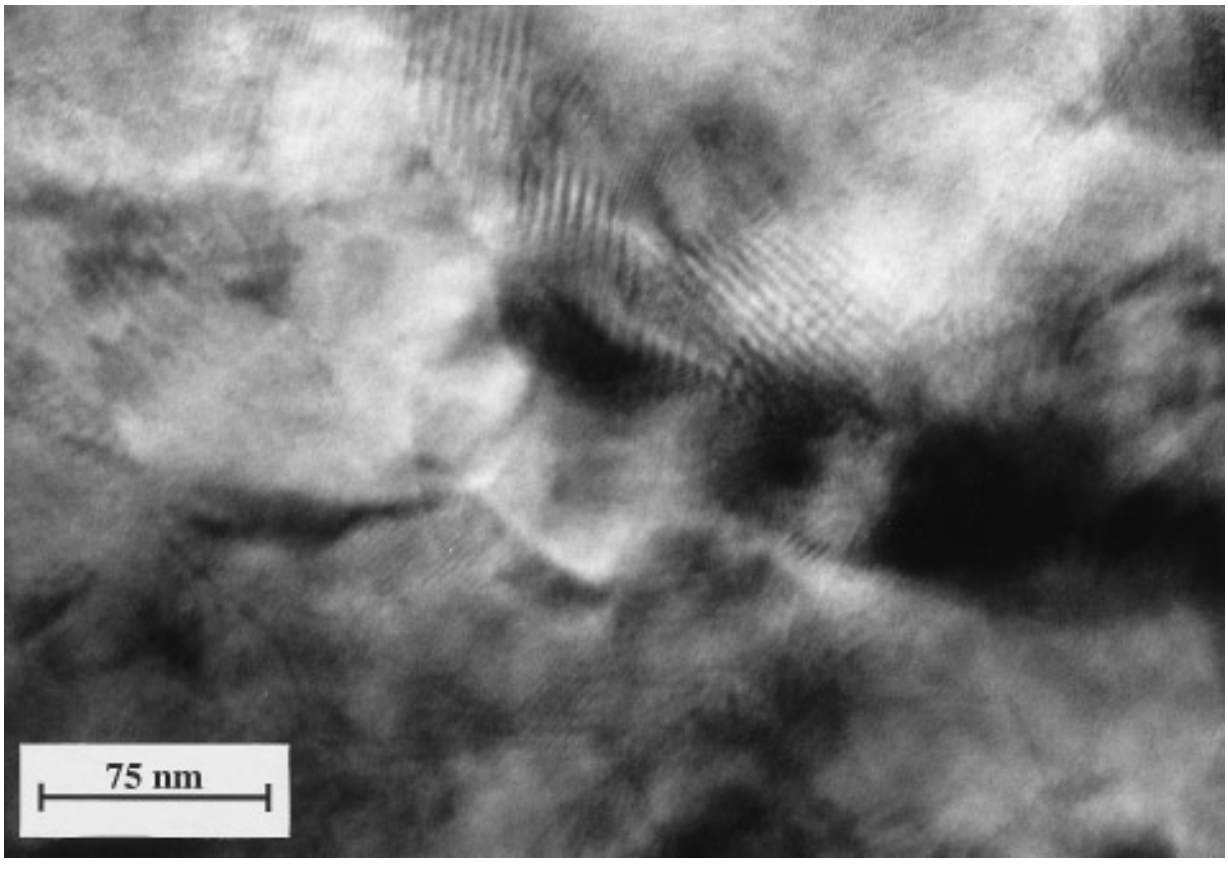

FIG. 1. Typical TEM micrograph of unmilled CuO showing distorted Moiré fringes, indicative of lattice strain.

fect structures of unmilled CuO were examined using a JOEL 4000FX transmission electron microscope (TEM) operating at 400 keV.

RESULTS

The microstructure of the unmilled CuO is shown in Fig. 1. The starting material is microcrystalline and the Moiré fringes are indicative of lattice strain. XRD patterns indicate that during the ball milling process, CuO peaks broaden and flatten within a short period of milling. The Fe peaks do not broaden noticeably before combustion but do begin to flatten following combustion (4). Figure 2 shows a typical Rietveld refinement of CuO and Fe, milled for 36 min. Rietveld refinement of samples milled to combustion show that the ADPs of oxygen in the CuO become very large, and then level out prior to combustion. Table 1 shows, for selected sample milling times, the refined unit cell and atomic coordinates of the phases, and the isotropic ADPs. Table 2 is a list of Bragg R factors and the point by point profile fitting index for the entire pattern (R_p value).

Anisotropic ADPs were refined for CuO, and these are given in Table 3. Crystal structures of the CuO unit cell (Fig. 3) were constructed from the Rietveld refinement of unmilled material (Figs. 3a and 3b), and the material milled for 36 min (Figs. 3c and 3d). These show the overall displacement of cations and anions within the structure. There is minor displacement of both species in unmilled material, and a high probability of displacement of O^{2-} ions in heavily milled material.

Raman spectra of unmilled material and material milled 36 min are shown in Fig. 4. The spectrum of unmilled material shows peaks at 294 and 595 cm^{-1}, corresponding to A_g and $B_g(z)$ modes (where A_g and $B_g(z)$ are the symmetric O translational modes in the y and z directions, i.e., along crystallographic b and c axes, respectively). The Raman bands were assigned with reference to a single crystal study (11). CuO milled 36 min shows Raman shifts of ca. 300 and 590 cm^{-1} for the respective modes. The vibrational frequencies observed in each case are essentially identical. This implies that the vibrational amplitudes are the same in milled and unmilled materials.

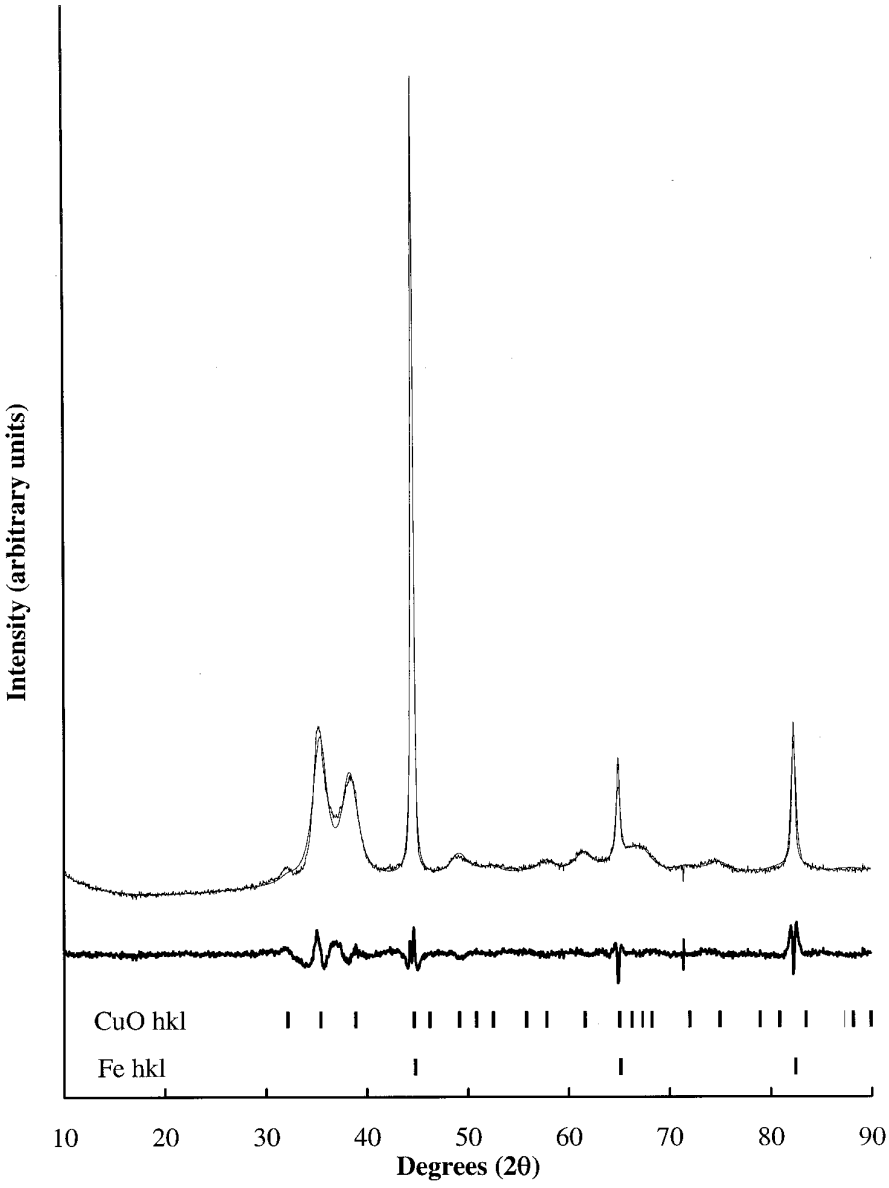

FIG. 2. Observed and calculated XRD traces of CuO and Fe powders prior to combustion (milled 36 min). The smooth line is the calculated pattern and the bold line is the difference pattern. The CuO peaks have broadened significantly while the Fe appears unchanged.

DISCUSSION

A. Method

The Rietveld technique is a method of crystal structure refinement which compares a calculated X-ray pattern to an experimental pattern made up of integrated profile intensities (12). ADPs are an integral part of the refinement procedure, as these reflect atomic movement within the crystal lattice. ADPs are time- and lattice-averaged probability density functions and are a measure of the mean square displacement of an atom from its ideal site (13). The atomic displacement affects the Madelung potential of the lattice at a given site. The Madelung potential, which is responsible for the cohesion of the ionic lattice, is the electrostatic potential on a test charge due to all other ions in the crystal.

Strain buildup in CuO during MA is seen in the cell dimension variations and with the variation in O atom positions with milling. The lattice strain is reflected in the atomic displacement parameters. The ADPs have components due to static disorder and thermal vibration of atoms. Thermal atomic motion is a low-energy process and doesn't contribute significantly to the nett lattice energy. However, true atomic displacements affect the lattice energy greatly

TABLE 1
Rietveld Refinement of Atomic Positions and Atomic Displacement Parameters for CuO and Fe from Unmilled Material through to Combustion

Milling time (min)	CuO unit cell (Å)				Oxygen y value	Fe unit cell (Å)	
	a	b	c	β (°)		a_0	B_{iso} (Å^2)
0	4.6832	3.4288	5.1297	99.3086	0.4281	2.8654	1.3600
10	4.6776	3.4593	5.1264	98.9645	0.4521	2.8652	1.5819
25	4.6839	3.4734	5.1226	98.7300	0.4721	2.8665	1.5481
30	4.6797	3.4768	5.1193	98,6440	0.4621	2.8657	1.5454
32	4.6844	3.4792	5.1215	98.6836	0.4469	2.8652	1.4836
34	4.6732	3.4770	5.1190	98.5625	0.4517	2.8659	1.2178
36	4.6791	3.4805	5.1183	98.5981	0.4523	2.8651	1.5260
37 (combustion)	4.6791	3.4805	5.1183	98.5981	0.4523	2.8705	0.7635

TABLE 2
Bragg R Factors and R_p Factors from Rietveld Refinements of CuO and Fe

Milling time (min)	CuO	Fe	Cu	Fe_3O_4	FeO	R_p
0	0.99	3.09	—	—	—	2.52
10	0.46	0.97	—	—	—	2.61
25	0.38	1.19	—	—	—	2.59
30	0.33	1.18	—	—	—	2.33
32	0.42	1.27	—	—	—	2.54
34	0.20	1.00	—	—	—	2.36
36	0.31	0.96	—	—	—	2.37
37	0.43	0.32	2.51	1.78	1.64	3.32

TABLE 3
Anisotropic ADPs for Cu and O in the CuO Lattice

Milling time (min)	Atom type	Anisotropic atomic displacement parameters					
		β_{11}	β_{22}	β_{33}	β_{12}[a]	β_{13}	β_{23}[a]
0	Cu	0.009	0.038	0.011	−0.004	0.006	−0.002
	O	0.013	0.015	0.030	—	−0.009	—
10	Cu	0.014	0.033	0.016	0.006	0.011	0.025
	O	0.136	0.006	0.082	—	−0.045	—
25	Cu	0.014	0.026	0.015	−0.003	0.010	0.027
	O	0.163	0.056	0.082	—	−0.059	—
30	Cu	0.010	0.026	0.015	0.001	0.011	0.024
	O	0.152	0.072	0.091	—	−0.069	—
32	Cu	0.014	0.028	0.010	0.018	0.005	0.038
	O	0.125	0.024	0.110	—	0.008	—
34	Cu	0.010	0.028	0.012	0.003	0.008	0.025
	O	0.153	0.015	0.109	—	−0.025	—
36	Cu	0.013	0.021	0.014	−0.009	0.012	0.021
	O	0.169	0.060	0.077	—	−0.073	—

[a] For oxygen atoms in the 4(e) site, β_{12} and β_{23} are fixed at zero (15).

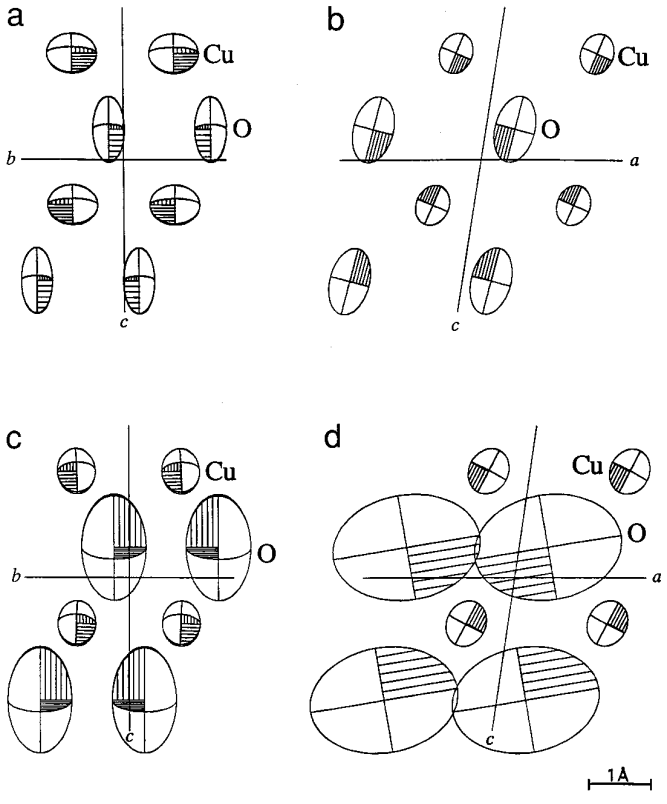

FIG. 3. Projected crystal structure of CuO with 95% probability ellipsoids showing ionic displacements. (a) 0 min milled ⟨100⟩ projection; (b) 0 min milled ⟨010⟩ projection; (c) 36 min milled ⟨100⟩ projection; (d) 36 min milled ⟨010⟩ projection.

by altering the Madelung potentials at selected sites. It is therefore necessary to differentiate between thermal vibration and static disorder of the oxygen atoms.

Dunitz *et al.* (14) have shown that the isotropic ADPs (B_{iso}) correspond to particular lattice vibrational modes for perfect crystals. The B_{iso} ought to reflect the vibrational frequency of a particular mode. The volumes covered by the ellipsoids in Fig. 3 represent the regions in which there is 95% probability of locating the atoms. The atoms may vibrate anywhere within that volume through thermal motion, or they may randomly occupy sites in that volume in a statically disordered structure. XRD at variable temperatures may be used to differentiate between the two causes for the ADP values (6). Alternatively, thermal vibrations may be discounted if the energies of the phonons are constant. The lattice vibrational modes observed in Raman spectra modes arise exclusively from O displacements along the *b* and *c* axes. Sizes of the Raman shifts may be related to the magnitude of the respective anisotropic ADPs (Table 3), i.e., β_{22} corresponds to A_g and β_{33} corresponds to $B_g(z)$ mode, where β_{ij} is the displacement parameter in the *ij* direction. Since the β_{22} and β_{33} values of milled material are nearly double those of the unmilled, large differences in the Raman shifts are expected if the ADPs merely reflect vibrational motion.

The Raman spectra of unmilled CuO and material milled 36 min (Fig. 4) indicate vibrational atomic displacements are nearly the same in each case. Therefore the excess values of the ADPs in milled CuO with respect to unmilled CuO may be assigned to static positional disorder. Static disorder and thermal vibration components of the ADPs of the unmilled material together may be considered as constant contributions to the ADPs in the rest of the (milled) materials.

The ADPs of highly crystalline CuO found by Åsbrink and Norrby (16) and later by Brese *et al.* (17) are in contrast with the values for the starting material found in this study. The generally larger isotropic ADPs found herein, and specifically the larger *a* and *c* axis components of the anisotropic ADPs in the highly milled material, indicate a more defective CuO sample was used here than in the earlier studies. This was confirmed by TEM (Fig. 1) and justifies the use of the present structure in subsequent calculations. Overall order in the *a* and *c* directions is degraded in unannealed material, which is reflected in the high values of the corresponding anisotropic ADPs (β_{ij}, Table 2).

Because Raman spectroscopy has shown that vibrational internal energy is constant throughout the series, a significant part of the structural energy (cohesive energy of the lattice) arises from nett electrostatic attraction and repulsion of ions. Nett electrostatic repulsive and attractive energy may be calculated from the Madelung potential of the lattice, which depends on interionic distances. The electrostatic energy (Madelung potential) U_M, is given by

$$U_M = -\frac{N_A z^2 e^2 M_L}{4\pi\varepsilon_0 r}, \qquad [1]$$

where N_A is Avogadro's number, z is the valency, e is the electron charge $= 1.602 \times 10^{-19}$C, ε_0 is the permittivity of free space, r is the interionic separation, and M_L is the Madelung constant, the geometric factor dependent on a particular lattice (18). For subsequent calculations, the lattice is approximated to an orthogonal system, with only displacement components along the principle axes being considered. It has been shown (14) that

$$\beta_{ij} = 2\pi^2 \overline{u}_{ij}^2 \mathbf{a}_i^* \cdot \mathbf{a}_j^*, \qquad [2]$$

where $\overline{u}_{ij}$ is the RMS displacement in the *ij* direction and $\mathbf{a}_i^*$ is the reciprocal lattice parameter in the *i* direction. Root mean square (RMS) displacements (as opposed to the mean in real space) may be calculated from the ADPs applied in calculations of RMS Madelung potential for the unmilled and the deformed lattices. Using Eq. [2], RMS displacements are found for O in each cell, given in Table

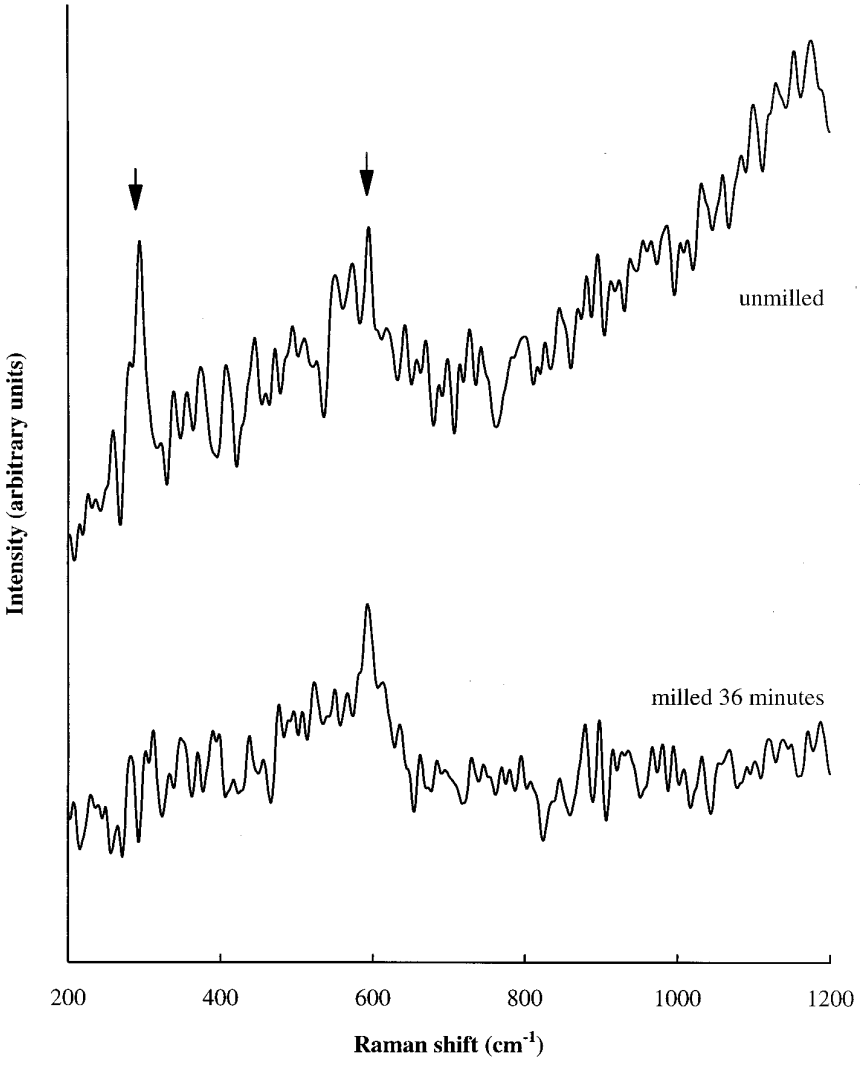

FIG. 4. Raman spectra of CuO, showing similar peak positions (arrowed) for both milled and unmilled material.

TABLE 4
RMS Principle Axis Displacements of Oxygen

Milling time (min)	Principle axis (Å)	ADP	Displacement real space $\bar{u}$ Å
0	a = 4.6832	β_{11} = 0.013	0.120
	b = 3.4288	β_{22} = 0.015	0.095
	c = 5.1297	β_{33} = 0.030	0.200
36	a = 4.6791	β_{11} = 0.169	0.433
	b = 3.4805	β_{22} = 0.060	0.192
	c = 5.1183	β_{33} = 0.077	0.320

Note. The strain indicated by cell dimension variation translates to energy by affecting the interionic distances.

4. If the most probable positions of loci of RMS displacements indicated by atomic coordinates and ADPs are considered to be occupied by static point charges, then lattice (Madelung) energies may be calculated (as in Table 5) for unmilled CuO and material milled just prior to reaction (36 min), using Eq. [1] and assuming divalent oxygen ions.

B. Implications for the Mechanism

Forrester and Schaffer (4) measured the activation energy for the reduction of CuO which reduced during milling from an initial value of 600 to 200 kJ/mole just prior to combustion. The precombustion value approximates the baseline destabilization of 223 kJ/mole (Table 5), due to inherent defects and thermal motion. The anion displacement accounts for a further 219 kJ/mole (Table 5). This is about half the difference between the initial and the

TABLE 5
Variation of Madelung Energy (U_M) of CuO Lattices with O Displacement

Milling time (min)	Oxygen location	U_M
0	O at most probable location	−3.011 MJ/mole
	O at RMS position	−3.234 MJ/mole
		ΔU_M = 223 kJ/mole
36	O at most probable location	−3.011 MJ/mole
	O at RMS position	−3.453 MJ/mole
		ΔU_M = 442 kJ/mole
	$\Delta U = \Delta U_{M2} - \Delta U_{M1}$ = 219 kJ/mole	

final activation energies; i.e., the lattice strain from displacements accounts for half the activation energy. Other crystalline defects, such as Schottky defects, dislocations, and grain boundaries would account for the remaining strain.

The O displacement also creates a diffusion pathway. Initially, the oxygen ADPs orient toward the ⟨0 0 1⟩ direction, and these change toward the ⟨1 0 0⟩ direction during milling. The copper ellipsoids are flattened in a plane away from the long principle axis of the oxygen ellipsoids, suggesting the Cu atoms move aside for (or are displaced by) the diffusion of the oxygen atoms. At combustion, the oxygen atoms can simply slide past the Cu atoms, leaving the Cu atoms in a face-centered cubic array (Figs. 3c and 3d). The Cu atoms in the C-centered lattice are related to their final positions in the F-centered lattice through two consecutive transformations, as follows:

$$\mathrm{C} \rightarrow \mathrm{I} \begin{pmatrix} 0 & 0 & \bar{1} \\ 0 & 1 & 0 \\ 1 & 0 & \bar{1} \end{pmatrix} \qquad \mathrm{I} \rightarrow \mathrm{F} \begin{pmatrix} 1 & 1 & 0 \\ \bar{1} & 1 & 0 \\ 0 & 0 & 1 \end{pmatrix}.$$

A monoclinic C-centered lattice is equivalent to a monoclinic I-centered lattice by redefinition of a principle axis along a basal diagonal (C → I). An F-centered lattice may be obtained from an I-centered one by rotation about a principle axis (I → F).

After the oxygen atoms have diffused out of the CuO lattice, they apparently diffuse into the Fe lattice. Prior to combustion Fe is strain-free (see Table 1), but following combustion, the Fe acquires strain. This lack of strain is seen in the lack of peak broadening in Fe_3O_4 and FeO which is produced in the combustion reaction. The acquired strain in Fe accounts for the peak shifts in its diffraction patterns following combustion (the cell dimension of Fe increases). The existence of FeO in ultrafine domains with Fe_3O_4, observed by Wang *et al.* (19), is suggestive of O mobility within these structures, consistent with the proposed mechanism of Fe oxidation. The cell dimension found for FeO is midway between that reported for FeO grown on Fe and FeO grown on Fe_3O_4 (20). FeO is therefore an intermediate stage to Fe_3O_4 formation from Fe.

The accumulated strain increases the lattice energy and decreases the activation energy required to initiate combustion. It also provides a diffusion pathway which effectively results in a movement of the reactants along the reaction coordinate toward the activated complex. The decreased activation energy barrier and the provision of a diffusion pathway provide the means by which a solid state reaction can occur at a significant rate at low temperatures.

It is apparent that some systems undergo a combustion reaction during milling while others do not. For example, Ag_2O and Al combust whereas ZnO and Ca do not, although the adiabatic temperature indicates that they should (21). Similarly, Ti and C combust to form a carbide whereas W and C do not (22). Since this work proposes a crystallographic mechanism for mechanical alloying induced reactions, it may become possible to define systems which suit the mechanical alloying process. It may be that suitable systems are those where the kinetic energy can be transformed into lattice strain energy in the form of atomic displacements and where the displacements are in a direction to facilitate atomic migration. This hypothesis remains to be tested.

CONCLUSIONS

1. It is possible to use crystallographically derived ADPs to visualize diffusion pathways for certain types of solid state reactions.
2. These ADPs are indicative of lattice strains which store energy (prior to reaction); i.e., the kinetic energy of milling is converted to chemical potential energy in the form of atomic displacement.
3. The anisotropic atomic displacement decreases the activation energy required for combustion and also provides an enhanced diffusion pathway.

ACKNOWLEDGMENTS

We thank Lou Rintoul and Tri Le of Queensland University of Technology for collecting the Raman spectra. The computer and photographic expertise of Peter Talbot and Rachel Hancock is greatly appreciated. This work is supported by the Australian Research Council.

REFERENCES

1. J. S. Benjamin, *Metall. Trans.* **1,** 2943 (1970).
2. G. B. Schaffer and P. G. McCormick, *Mater. Forum* **16,** 91 (1992).
3. B. J. M. Aikin, T. H. Courtney, and D. R. Maurice, *Mater. Sci. Eng. A* **147,** 229 (1991).

4. J. S. Forrester and G. B. Schaffer, *Metall. Trans. A* **26,** 725 (1995).
5. M. C. Favas, J. MacB. Harrowfield, D. L. Kepert, B. W. Skelton, L. M. Vitolo, and A. H. White, *Aust. J. Chem.* **45,** 1547 (1992).
6. D. N. Argyriou, *J. Appl. Crystallogr.* **27,** 155 (1994).
7. H. M. Rietveld, *J. Appl. Crystallogr.* **2,** 65 (1969).
8. R. J. Hill and C. J. Howard, Report No. M112, Australian Atomic Energy Commission, Sydney, Australia, 1986.
9. F. Izumi, *in* ''The Rietveld Method'' (R. A. Young, Ed.), Chap. 13, Oxford Univ. Press, Oxford, 1993.
10. Y.-I. Kim and F. Izumi, *J. Ceram. Soc. Jpn.* **102,** 401 (1994).
11. H. Hagemann, H. Bill, W. Sadowski, E. Walker, and M. François, *Solid State Comm.* **73,** 447 (1990).
12. R. A. Young (Ed.), ''The Rietveld Method.'' Oxford Univ. Press, Oxford, 1993.
13. G. H. Stout and L. H. Jensen, ''X-ray Structure Determination—A Practical Guide,'' p. 424. Macmillan, London, 1983.
14. J. D. Dunitz, V. Schomaker, and K. N. Trueblood, *J. Phys. Chem.* **92,** 856 (1988).
15. W. J. A. M. Peterse, and J. H. Palm, *Acta Crystallogr.* **20,** 147 (1966).
16. S. Åsbrink and L.-J. Norrby, *Acta Crystallogr. B* **26,** 8 (1970).
17. N. E. Brese, M. O'Keeffe, B. L. Ramakrishna, and R. B. Von Dreele, *J. Solid State Chem.* **89,** 184 (1990).
18. R. M. Rosenberg, ''Principles of Physical Chemistry,'' p. 461. Oxford Univ. Press, New York, 1977.
19. Y. G. Wang, D. H. Ping, and J. G. Guo, *J. Appl. Crystallogr.* **27,** 96 (1994).
20. R. W. G. Wyckoff, ''Crystal Structures,'' 2nd ed, Vol. 1, p. 87. Interscience, New York, 1965.
21. G. B. Schaffer and P. G. McCormick, *Metall. Trans. A* **22,** 3019 (1991).
22. G. Le Caër, E. Buer-Grosse, A. Pianelli, E. Bouzy, and P. Matteazzi, *J. Mater. Sci.* **25,** 4726 (1990).